Ceramics International 51 (2025) 9669–9676

Contents lists available at ScienceDirect

Ceramics International

journal homepage: www.elsevier.com/locate/ceramint

Original research article

Synthesis and annealing effects on microstructure and optical properties of wide-bandgap polycrystalline ferro-pseudobrookite $FeTi_2O_5$ sol-gel layers

Maria Cristina Ferrara [a,*], Marco Montecchi [b], Alberto Mittiga [b], Monica Schioppa [a], Saverio Mazzarelli [a], Leander Tapfer [a,1], Nico Lovergine [c,**], Paola Prete [c]

[a] ENEA National Agency for New Technologies Energy and Economic Sustainable Development, Department for Sustainability, Brindisi Research Centre, 72100, Brindisi, Italy

[b] ENEA National Agency for New Technologies Energy and Economic Sustainable Development, Energy Technologies and Renewable Sources Department, Casaccia Research Centre, 00123, Rome, Italy

[c] Department of Innovation Engineering, University of Salento, Via Monteroni, 73100, Lecce, Italy

ARTICLE INFO

Keywords:
Ferropseudobrookite
Sol-gel synthesis
Thin films
Ceramic coatings
Optical properties

ABSTRACT

Wide bandgap (WBG) and high thermal stability pseudobrookite compounds, $Fe_{1+x}Ti_{2-x}O_5$ ($0 \leq x \leq 1$), are promising materials for photocatalysis, high-temperature thermoelectric applications, green production of hydrogen by water splitting, fabrication of power electronics, and optoelectronic devices. Here, we report on WBG, polycrystalline, ferropseudobrookite, $FeTi_2O_5$, coatings, stable at high temperature, prepared by an optimized sol-gel route on fused silica and silicon substrates. The chemical composition, the amorphous-to-crystalline phase transformation, and the influence of the annealing temperature and atmosphere (air and argon) on the formation and evolution of the crystalline phases were investigated in detail by combining thermogravimetric and differential scanning calorimetry analysis with Fourier-transform infrared spectroscopy and X-ray diffraction. The experimental results clearly show that orthorhombic $FeTi_2O_5$ single phase develops in the interval 500–560 °C (crystalline domain size about 16 nm at 560 °C). The coatings remain in a single $FeTi_2O_5$ phase up to a temperature of about 590 °C. At higher temperatures, a rutile-TiO_2 secondary phase is formed, both in an oxidizing and inert atmosphere, while the ferropseudobrookite phase remains unchanged. The results suggest that the secondary phase arises from the presence of superficial Ti-O- dangling bonds that at temperatures above 590 °C begin to arrange themselves to form polycrystalline rutile-TiO_2 (crystalline domain size ≈8 nm at 620 °C). The results also show that the average energy required to break the Ti-O-Ti molecular bonds of the $FeTi_2O_5$ phase increases with temperature, improving its thermal stability. Optical absorption spectroscopy measurements carried out on coatings heated at 560 °C, yield an optical bandgap of about 2.25 eV, a refractive index of about 1.84 at 550 nm, and a weak UVC positive band, peaked at about 5.9 eV, on transmittance that disappears when the samples are annealed at 750 °C.

1. Introduction

In the last decade, pseudobrookite $Fe_{1+x}Ti_{2-x}O_5$ ($0 \leq x \leq 1$) compounds have been the topic of several research studies devoted mainly to material synthesis and fabrication, and functional properties [1–30]. The increased scientific and technological interest in pseudobrookite powders and films is triggered by high thermal and aqueous stability [1], the tunable electrical and ferromagnetic properties [2], a high Seebeck coefficient [2] and a wide band gap (around 2 eV) [1,12,13,21] with band level positions close to the H_2O redox levels that make them more favorable for driving water splitting reactions compared to hematite [1,17–28]. Consequently, these properties and features make pseudobrookite-based materials very interesting for applications in photocatalysis and photovoltaics [1,17–27], and for potential implementations in various advanced optoelectronic, electromagnetic, thermoelectric, spintronic and sensor devices [1–16]. Very recently, single phase pseudobrookites materials, especially pure Fe_2TiO_5 films, have been developed and studied as promising candidates for designing the

* Corresponding author.
** Corresponding author.
E-mail addresses: cristina.ferrara@enea.it (M.C. Ferrara), nico.lovergine@unisalento.it (N. Lovergine).
[1] present address: Department of Innovation Engineering, University of Salento, Via Monteroni, 73100 Lecce, Italy.

https://doi.org/10.1016/j.ceramint.2024.12.397
Received 31 October 2024; Received in revised form 20 December 2024; Accepted 24 December 2024
Available online 25 December 2024

next generation of water splitting photoelectrodes for green hydrogen production [1,16–27]. Furthermore, pure titanium-rich and single-phase polycrystalline ferro-pseudobrookite, $FeTi_2O_5$, with a highly ordered Fe^{2+}/Ti^{4+} occupation, is attracting interest as a spin Jahn-Teller material for fundamental studies of antiferromagnetic phase transitions, magnetoelastic coupling and quasi-1D magnets and muons decay [29,30].

Although Fe_2TiO_5 and $FeTi_2O_5$ single phase materials are of scientific and technological interest, studies on their synthesis, structure, and morphological characterization are limited in the literature. Furthermore, few investigations have focused on their optical, electrical, and magnetic properties [10,12,13,16,17,28–30]. This is particularly the case of the pure ferrous $FeTi_2O_5$ pseudobrookite phase material synthesized as thin solid films. The reason may be related to the difficulty in eliminating the presence of impurity phases in natural pseudobrookites and to synthesize pure and clean ferric- and ferrous-pseudobrookite single phases without the occurrence of other phases such as hematite (Fe_2O_3), ilmenite ($FeTiO_3$) and rutile-TiO_2 secondary phases [1,3,4,15,31].

In the present work, the influence of the annealing temperature on the evolution of the chemical and microstructural characteristics of the $FeTi_2O_5$ coatings heat-treated up to 950 °C was studied. In particular, the results of the characterizations performed to investigate the amorphous-to-crystalline phase transformation, which develops $FeTi_2O_5$ crystals, are reported and discussed, along with the underlying causes leading to the formation of secondary phases. Moreover, the optical properties, specifically the complex refractive index and the energy gap, of spin-coated $FeTi_2O_5$ layers grown on fused silica substrates were investigated and correlated to the film structure. As far as we know, the published studies on the physical properties of $FeTi_2O_5$ mainly regard magnetic and electric properties [11,15,29,30] and no study has been published yet on its optical properties.

Since materials grown by sol-gel routes involves hydrolysis, oxidation, and decomposition processes [4], the suitable temperature to grow single phase $FeTi_2O_5$ coatings and the formation of secondary phases were investigated by combining thermo-gravimetric analysis (TGA) and differential scanning calorimetry (DSC) with Fourier-transform infrared spectroscopy (FTIR) and X-ray diffraction (XRD). For this purpose, the thermal analyses of sol-gel powders were performed in a large interval of temperature, 25–1150 °C, and the endothermic and exothermic features in the DSC curve were correlated to the changes in the TG curve and to the variations of structure of coatings annealed up to 950 °C.

To study the influence of the oxygen on the features in DSC curve related with the formation of the $FeTi_2O_5$ crystalline phase and the appearance of the secondary phase, thermal analyses both under oxidizing (air) and inert (argon) atmosphere were performed, in the range 500–1150 °C. The crystalline phases of the powders were then analyzed by XRD analysis.

The paper is organized as follows: after the introduction, the synthesis procedure, the film deposition, and the characterization techniques are described in Section 2. The experimental results are reported and discussed in the subsections of Section 3, including thermal behavior (1), surface morphology (2), crystallographic structure and chemical bonds evolution (3), along with optical measurements (4). The summary and conclusions are given in Section 4.

2. Experimental details: sample preparation and characterization techniques

2.1. Sol-gel synthesis

The sol-gel precursor solution (molar ratio Fe:Ti = 1:2) was prepared following the procedure reported in our previous paper [4] using, as solvents and reagents, iron(III) chloride hexahydrate (Sigma-Aldrich, ACS grade) and titanium tetraisopropoxide, TTIP, (Sigma-Aldrich, ≥97.0 % purity) respectively as precursor of titanium and iron, acetylacetone, AcAc, (Sigma-Aldrich, ≥99.5 % purity), as chelating agent of TTIP, HCl (30 %) as acid catalyst of the hydrolysis/condensation reaction of the alkoxide groups, ethanol, EtOH, (Sigma-Aldrich, ≥99.9 % purity), and isopropyl alcohol, IPA, (Sigma-Aldrich, ≥99.9 % purity). To sum up briefly, a 0.35M solution of Fe (III) chloride hexahydrate dissolved in a mixture of water-ethanol (molar ratio H_2O/EtOH = 1:1) was added drop by drop to an HCl-catalysed solution (pH ≈ 5) prepared using TTIP, AcAc, and IPA, in the molar ratio TTIP:AcAc = 1:2 and TTIP:IPA = 1:20 [4]. A concentrated ammonium hydroxide solution (30 %) was added to adjust the pH in the range of 4.5–5.0, to avoid precipitation and gel formation. The solution was then kept under stirring for 24 h. The coatings were prepared in a glove box by depositing the colloidal sol-gel solution on double-side polished fused silica and (100)-Si substrates under a mixed atmosphere of air and dry nitrogen at about 23 °C and 30 % relative humidity. Thin layers were deposited by a controlled spin-coating technique (1600 RPM of spinning speed for 30 s) to roll out the solution homogeneously on surface substrates, while thicker layers were obtained by the drop-casting method. The coatings were then dried in the air at 80 °C for 2 h to get the evaporation of adsorbed water and solvents, heated up to 500 °C in air to favor the reactions of polycondensation with the elimination of hydroxyl and organic groups, and annealed in the range 500–950 °C to investigate the influence of temperature on the coating's properties.

2.2. Characterization techniques and methods

The Thermogravimetric, TG, and DSC measurements were carried out on sol-gel powders by using a thermal analyzer (TA Instruments Q600, Delaware, USA) in the temperature range 25–1150 °C, at a heating scan rate of 5 °C/min in two different dynamic atmospheres: air and argon. The powders were obtained by drying the precursor solutions at 80 °C in air for 10 h.

The morphological investigations of sol-gel films deposited onto (100)-Si wafer substrates were performed by field-emission scanning electron microscopy (FESEM) using a Sigma VP (Zeiss, Oberkochen, Germany) microscope equipped with a Gemini-1 electron column and a primary electron beam energy of 10 keV.

The structure of the coatings was analyzed by means of a 3 kW single-crystal X-ray diffractometer (Philips PW1880, Eindhoven, The Netherlands) equipped with a Cu-target X-ray source ($\lambda = 0.154$ nm), a proportional counter as X-ray detector, and a post-sample flat graphite crystal and a parallel-beam-plate collimator to reduce the background scattering. The configuration of the X-ray instrument was optimized for microstructural analysis of thin and ultrathin films and powders. All the XRD patterns were recorded by 2θ scans (range 10–80° and angular step size of 0.02°) of the post-sample monochromator-detector system and keeping the incident angle between the impinging x-ray beam and the sample surface constant throughout the measurements, i.e. $\omega_i = 1.0°$.

The nature of the chemical-bonds and their evolution with the temperature were investigated by means of FTIR measurements performed on coatings grown by drop-casting method on (100)-Si substrates. The spectra of the samples and of a bare (100)-Si substrate (used as background spectrum) were recorded from 256 scans at a resolution of 2 cm^{-1} in the mid-infrared (4000–400 cm^{-1}) region using a FTIR spectrophotometer (Cary 600 series, Agilent Technologies, Santa Clara (CA), USA) equipped with a KBr/Ge beam splitter, a DTGS detector and a purge air system to continually remove H_2O vapor and CO_2. Since annealing induces the formation of silicon oxides on the uncovered surface of Si-wafers [32], the silicon substrate was heated at the same temperatures as the analyzed sample to subtract the infrared absorptions of SiO_x oxides from the IR spectra of the coatings.

For the optical characterization, hemispherical spectrophotometric measurements of transmittance, $T_n(\lambda)$, film side reflectance, $R_n(\lambda)$, and substrate side reflectance, $R_s(\lambda)$, were performed with the PerkinElmer Lambda 950S spectrophotometer, equipped with a 150 mm diameter

integrating sphere. A black cardboard mask with a 20 mm opening diameter was used on the port of the integrating sphere dedicated to the measurement of hemispherical reflectance to ensure good positioning of the samples. The measurements were performed on samples obtained depositing the sol-gel solution on fused silica substrates. The refractive index and the extinction coefficient of the samples annealed at 560 °C and 750 °C were determined with the KSEMAW open-source software [33]. The energy gap was graphically estimated starting from the optical absorption coefficient calculated from the extinction coefficient curves.

3. Results and discussion

3.1. Thermal behavior of the ferropseudobrookite precursor powder

Thermogravimetric and DSC measurements were simultaneously performed to investigate the thermal behaviour of sol-gel powders both under oxidizing (air) and inert (argon) atmosphere, as shown in Fig. 1. TG-DSC curves recorded in air flux in the range 25–1150 °C are reported in Fig. 1 (a), while the TG-DSC curves obtained in air flux from 25 °C to 500 °C and in argon flux in the interval 500–1150 °C are shown in Fig. 1 (b).

In the range 25–500 °C, both TG curves of Fig. 1 (a) and (b) show two distinct weight losses. The first weight loss, up to 115 °C, associated with the endothermic peak at 52 °C in the DSC curves, represents the removal of the physically adsorbed water [34]. The second loss, appearing in the interval 120–480 °C, is associated both with the endothermic reaction peaked at around 176 °C and with the two exothermic reactions peaked at 238 °C and at 382 °C. The endothermic peak at 176 °C can be ascribed

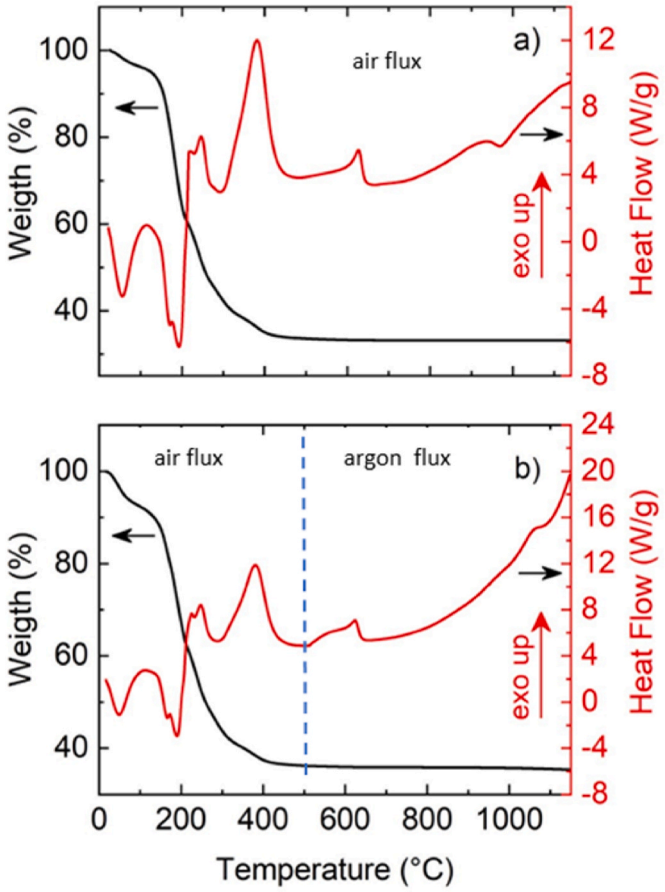

Fig. 1. TG-DSC thermograms of sol-gel powders obtained from the precursor sol-gel solution carried out from 25 °C to 1150 °C in air flux (a) and in air flux from 25 °C to 500 °C and argon flux in the interval 500 °C–1150 °C (b).

to the loss of small molecular compounds, such as bound water [34] and alcohols, from the xerogel structure, whereas the two exothermic reactions at 238 °C and at 382 °C can be associated to the cross-linking reactions leading to the formation of the sol-gel oxide accompanied by the release of OH and alkyl groups [4].

Above 480 °C, both in air and argon flux, the flatness of the weight loss curves indicates that no more exothermic or endothermic reactions associated with detectable weight loss occur [4]. This is confirmed by the FTIR analysis showing the absence of organic and hydroxyl groups in the spectrum of the sample heat-treated at 500 °C [4].

In the temperature range 480–1150 °C the DSC curve recorded in air flux (Fig. 1a) shows two exothermic features. The first, in the interval 480–650 °C, is characterized by a

positive tail, starting at about 490 °C, and by a peak at about 620 °C with an extrapolated onset temperature, T_{onset}, of about 590 °C. The absence of loss weight and the presence of two onset temperatures suggests that this feature is due to presence of two crystallization reactions. This is confirmed by our XRD results demonstrating the formation of $FeTi_2O_5$ crystalline phase at 560 °C and the formation of rutile-TiO_2 at 620 °C (see Section 3.3). The second exothermic feature, in the interval 750–1150 °C, shows the presence of a maximum at about 940 °C and is characterized by a very slow variation of the enthalpy and release of energy in the form of heat. These two exothermic features are also observed in the DSC acquired in argon flux in the range 500–1150 °C (Fig. 1b). However, the release of energy in the range 750–1150 °C under the argon atmosphere grows exponentially and is about four times greater than that in air and the (energy peak) maximum is shifted to a higher temperature, about 1060 °C.

The nature of the enthalpy changes observed in the temperature range 500–1150 °C was investigated by means of XRD and FTIR (see Section 3.3) measurements carried out on sol-gel coatings annealed in air at 500 °C, 550 °C, 555 °C, 560 °C, 580 °C, 620 °C, 750 °C, and 950 °C. Different annealing temperatures were chosen in the interval 500–620 °C because the shape of the first exothermic feature suggests the presence of more than one crystallization process.

3.2. Surface morphology

Morphological analysis performed on sol-gel coatings deposited by spin-coating methods showed that the developed $FeTi_2O_5$ sol-gel films do not form continuous and uniform coatings, and the substrate (Si wafer or silica) is not completely covered. As in the case of dip-coated deposited layers [4], the irregular coverage gives rise to a fractal-like pattern structure of the deposited film [4] and has been observed immediately after the film deposition, before the drying and sintering processes [4]. The chemical treatment of the substrate surface prior to deposition, i.e. hydrophilic or hydrophobic substrate surface, does not influence the surface morphology of the deposited films.

A high-magnification in-lens FESEM cross-sectional image of a thin $FeTi_2O_5$ film deposited on a (100)-Si wafer substrate by drop casting and annealed at 560 °C is shown in Fig. 2. The $FeTi_2O_5$ coating covering the substrate is of uniform thickness and exhibits a homogeneous and compact structure formed by close-packed crystallites with an average size of about 16 nm, as estimated by XRD analyses in Section 3.3. Within the FESEM resolution, no porosity or film fractures can be observed.

3.3. Crystallographic structure and chemical evolution

The XRD patterns recorded for different annealing temperatures of the sol-gel solution deposited onto (100)-Si wafer clearly show that crystallization and phase evolution take place in the ferro-pseudobrookite layers at processing temperature (Fig. 3). The amorphous structure of the deposited sol-gel solution can be observed up to a temperature of 555 °C, although very weak diffraction peaks, (110) and (023) Bragg peaks, of the ferro-pseudobrookite begin to appear at 500 °C. At 560 °C no amorphous peaks are visible anymore and only the

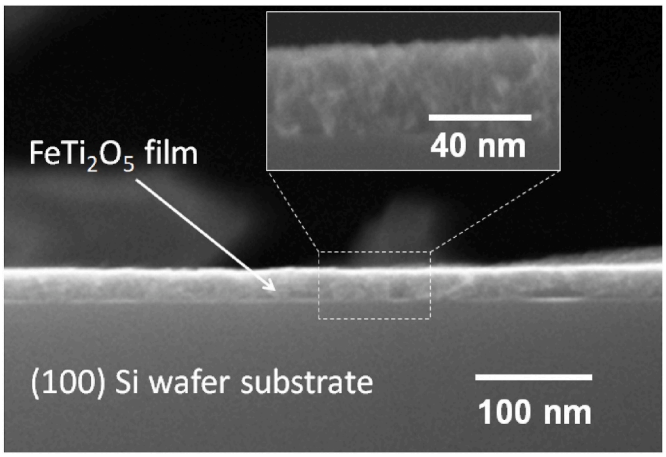

Fig. 2. In-lens FESEM images (20 keV) of a 40 nm thick $FeTi_2O_5$ coating deposited by drop-casting onto (100)-Si wafer and annealed at 560 °C in air.

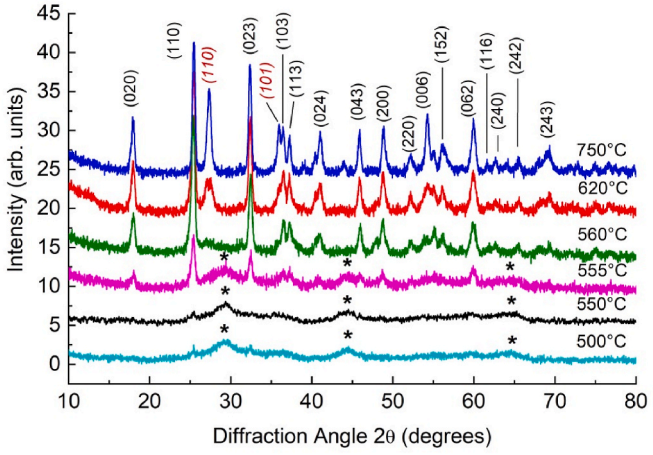

Fig. 3. Glancing incidence XRD patterns of the sol-gel solution deposited onto (100)-Si wafer, recorded after annealing at various temperatures. At an annealing temperature of 560 °C, only the ferro-pseudobrookite $FeTi_2O_5$ (ICDD card n. 76–2372) phase is observed, while the amorphous phase (indicated by *) is vanished. At a temperature of 620 °C the rutile phase of titania (ICDD card n. 88–1175), indicated by cursive Miller indices, appears and evolves further at a temperature of 750 °C.

Bragg peaks belonging to the orthorhombic phase of the ferro-pseudobrookite $FeTi_2O_5$ [35,36] are observed in accordance with the ICDD card n. 76–2672 [37]. The crystallographic unit cell (space group: Cmcm) of the orthorhombic $FeTi_2O_5$ has the lattice parameters: a = 0.3756 nm, b = 0.9812 nm and c = 1.0093 nm [37]. Further increasing the temperature, at 620 °C the (110) Bragg peak, attributed to the rutile phase of titania (ICDD card n. 88–1175) [37] starts to appear, while the ferro-pseudobrookite phase remains stable. At 750 °C the rutile phase is more pronounced and the (101) Bragg peak is well observed. In summary, the orthorhombic $FeTi_2O_5$ phase develops in the annealing temperature range 500–560 °C and the rutile-TiO_2 secondary phase is formed after further increasing the annealing temperature. This agrees with the DSC results which show the onset temperature of the tail of the first exothermic feature at 490 °C and the peak at 620 °C, which can be associated, respectively, with the starting temperature of the crystallization process of $FeTi_2O_5$ phase and to the maximum of the crystallization peak of the rutile-TiO_2 phase. As a result of XRD and DSC analysis, it is also reasonable to believe that the development of the secondary phase starts around 590 °C, that is, the extrapolated onset temperature of the peak observed at 620 °C on the DSC curve.

The average size of the ferro-pseudobrookite crystallites, as estimated by using the Scherrer's equation and line fitting with Voigt function [4] of the (110) and (023) Bragg peaks, increases almost linearly from 16 nm at 555 °C to about 20 nm at 750 °C. The crystallite size of the rutile phase increases from 8 nm at 620 °C to 15 nm at 750 °C.

The X-ray diffraction patterns of the powders heated by the thermal analyzer up to 1150 °C in both oxidizing (air) and inert (argon) atmospheres are shown in Fig. 4. The patterns clearly show the sole presence of Bragg peaks attributed to the $FeTi_2O_5$ and the rutile-TiO_2 phases. This finding suggests that the oxygen presence has no role in the microstructure changes of $FeTi_2O_5$ and that, therefore, the formation and growth of rutile-TiO_2 species is due to the annealing process and not to oxygen presence.

This agrees with the DSC analyses showing the presence of the peak at 620 °C, attributable to the formation of the rutile-TiO_2 phase, in both DSC curves shown in Fig. 1. This finding suggests that the oxygen presence has no role in the formation of rutile-TiO_2 species, whose formation is attributable to annealing treatments carried out at temperatures above 590 °C (onset temperature of the exothermic peak at 620 °C).

In summary, the DSC and XRD experimental results clearly show that the orthorhombic $FeTi_2O_5$ phase develops in the annealing temperature interval of 500–560 °C. The coatings remain in a single $FeTi_2O_5$ phase up to a temperature of about 590 °C. Further increasing the annealing temperature, the nucleation process of the rutile-TiO_2 begins, under both oxidizing and inert atmosphere, while the ferro-pseudobrookite phase remains unchanged.

The XRD results agree with the FTIR analyses carried out on annealed samples in the interval 500–950 °C with the aim of investigating the chemical bond changes of $FeTi_2O_5$ coatings induced by heat treatments.

Fig. 5 shows the FTIR spectra of a sample annealed in air at seven different temperatures, 500, 560, 580, 620, 750, 850, and 950 °C. Since no infrared absorptions of the sol-gel coatings were observed in the spectral region 4000-1150 cm^{-1} after annealing at 500 °C (see Fig. 2 in Ref. [4]), only the region 1000-400 cm^{-1} is reported in Fig. 5. In the region 1000 - 400 cm^{-1}, where Ti-O and Ti-O-Ti molecular bonds absorb [38–43], a large multi-peaked absorption can be observed located at around 500 cm^{-1}. Since chemical environments influence the features in the infrared spectrum, especially, the peak positions and their intensities [42], it is reasonable to believe that the multi-peaked band is constituted by overlapped vibrational modes of Ti-O and Ti-O-Ti bonds with different local chemical environments surroundings Ti and O atoms and,

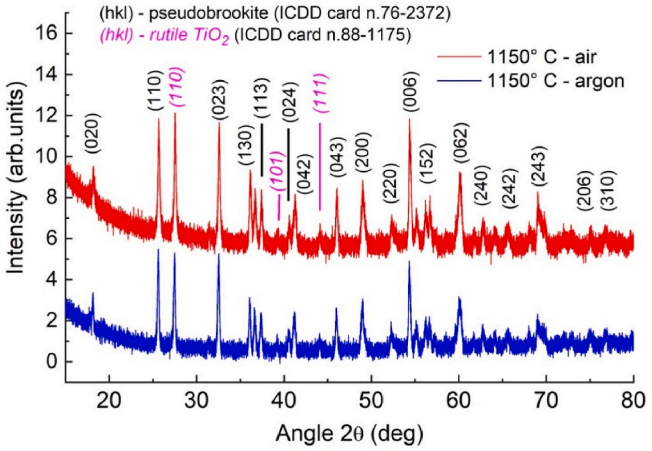

Fig. 4. XRD patterns of the powders heated with the thermal analyzer from 25 °C to 1150 °C in air (red) and argon (blue). Both XRD patterns exhibit the characteristic and most intense Bragg peaks of the rutile TiO_2 phase. (For interpretation of the references to colour in this figure legend, the reader is referred to the Web version of this article.)

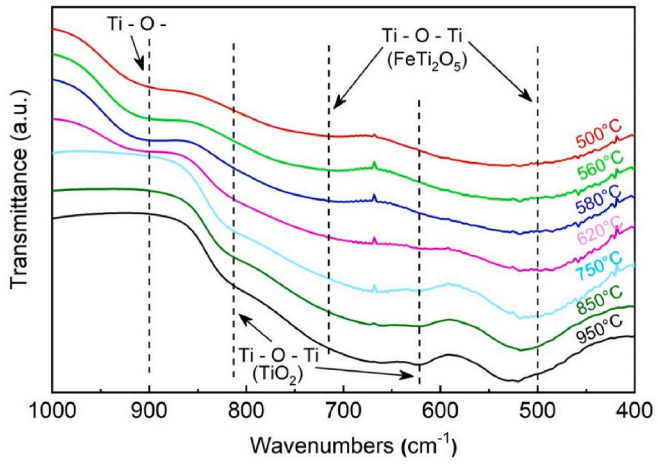

Fig. 5. FTIR spectra of the sol-gel solution deposited onto the (100)-Si wafer recorded after annealing at various temperatures. The possible assignments of the absorption bands are also reported. At annealing temperatures up to 580 °C, the absorption bands can be assigned to Ti-O-Ti bonds of the $FeTi_2O_5$ phase and Ti-O- dangling bonds. At a temperature of 620 °C, the Ti-O- band begins to decrease until it disappears completely at T ≥ 750 °C, while the rutile-TiO_2 bonds appear and further evolve with temperature.

consequently, different bonds strength [4,39–43]. The comparison among the infrared spectra clearly shows that the multi-peaked band changes and evolves with the temperature.

At 500, 560, and 580 °C, the large broad absorption band shows the presence of two shoulders at around 900 and 715 cm^{-1}, the first one ascribable to Ti-O- vibrations with the oxygen atom in the non-binding conditions [38,39], whereas the second one along with the peak around 500 cm^{-1} may be assigned to Ti-O-Ti vibrations [39–43]. Based on our XRD results, the Ti-O-Ti absorptions can be ascribed to both amorphous (spectrum at 500 °C) and polycrystalline ferro-pseudobrokite phases (spectra at 560 and 580 °C). Increasing the temperature, the shoulder at 900 cm^{-1} decreases at 620 °C and disappears at T ≥ 750 °C. At the same time, two new shoulders, around 815 and 622 cm^{-1}, appear. In agreement with literature [39–43] and on the base of our XRD results, that clearly show the presence of rutile-TiO_2 diffraction peaks at T ≥ 620 °C, these two new absorptions may be assigned to Ti-O-Ti vibrations of rutile-TiO_2.

The formation of TiO_2 oxides by the annealing process has been already observed in $SrTiO_3$ perovskites and attributed to the presence of defective structures, specifically to the segregation of Ti and O on the surface of $SrTiO_3$ [44–46]. The disappearance of Ti-O- band in conjunction with the appearance of rutile-TiO_2 absorptions, in our FTIR spectra, allow us to suppose that the formation of the rutile-TiO_2 phase could arise from the segregation of surface Ti-O- species that organize to form polycrystalline rutile-TiO_2.

Noteworthy, by increasing the temperature, the Ti-O-Ti peak around 500 cm^{-1} shifts towards higher energies, shrinks, and increases in intensity. These changes are more evident after annealing at temperatures ≥750 °C. The narrowing of the Ti-O-Ti peak can be ascribed to the fact that local chemical environment surrounding Ti and O atoms become more and more similar [42], leading to more homogeneous and ordered arrangements of bonds and atoms within the $FeTi_2O_5$ structure. The blue shift of the absorption suggests that increasing the temperature increases the average energy required to break the Ti-O-Ti molecular bonds, increasing, consequently, the thermal stability of $FeTi_2O_5$ unit cells and crystallites. These findings are supported by the results of our DSC analysis. In the DSC curves reported in Fig. 1, indeed, in the range 750–1150 °C, the decrease in enthalpy with the temperature indicates a greater degree of stability of the chemical structure.

In summary, in agreement with our XRD and DSC analyses, the experimental FTIR results suggest that the rutile-TiO_2 secondary phase could arise from the presence of surface Ti-O- dangling bonds which, owing to annealing performed at temperatures higher than 590 °C, rearrange themselves to form rutile-TiO_2 species. In agreement with DSC results, the FTIR analyses also suggest that for annealing temperature ≥750 °C, the thermal stability of the Ti-O-Ti chemical bonds of $FeTi_2O_5$ increases with temperature.

3.4. *Optical characterization: temperature evolution of optical parameters and band-gap energy*

The influence of the annealing temperature on the optical parameters and the energy gap of $FeTi_2O_5$ was investigated by spectrophotometric measurements at normal incidence of the hemispherical transmittance $T_n(\lambda)$ and reflectance $R_n(\lambda)$ of a sample annealed at 560 and 750 °C. The transmittance data are reported in Fig. 6 together with the direct transmittance of the sample heated at 750 °C.

In the UV region, transmittance never goes to zero (Fig. 6), reaching a minimum value of about 20 % and 10 %, respectively for hemispherical and direct measurements, showing that light scattering is occurring.

The transmittance of the sample treated at 560 °C shows a weak positive band that peaked at about 5.9 eV (210 nm), which vanishes after annealing at 750 °C. A similar UVC band can be observed as a negative band, peaked around 225 nm (5.5 eV), in the UV–VIS absorbance spectrum of almost pure Fe_2TiO_5 powders as recently reported in literature [47]. The origin of this transmittance positive band in the UVC region of ferro-pseudobrookites, is still not clear and not well understood. Further investigations are necessary to study and clarify the origin of the transmittance positive band.

Since the transmittance measurements involve an area of several squared millimeters, considering that the film does not completely cover the substrate (see Section 3.2), the measured transmittance, $T_n(\lambda)$, is the result of the mix of the hemispherical transmittances arising from the bare substrate, $T_s(\lambda)$, and from the substrate covered by of $FeTi_2O_5$ film, $T(\lambda)$:

$$T_n(\lambda) = p\,T(\lambda) + (1-p)\,T_s(\lambda) \quad (1)$$

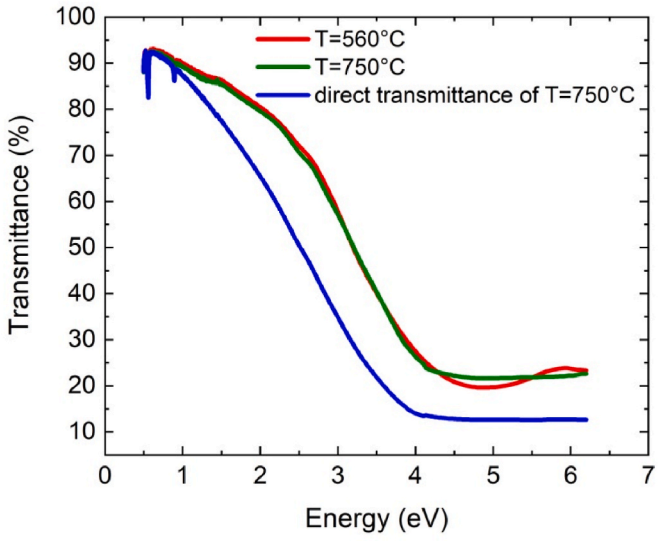

Fig. 6. Energy dependence of the hemispherical transmittance spectra, T_n (eV), of a sample heat treated at 560 °C (red curve) and 750 °C (green curve). The direct transmittance (blue curve) of the sample heated at 750 °C is reported, too. The transmittances do not go to zero, because the substrate is not completely covered by the coating. (For interpretation of the references to colour in this figure legend, the reader is referred to the Web version of this article.)

where p and (1-p) are, respectively, the portion of the substrate surface covered and uncovered by $FeTi_2O_5$. An analogous equation can be written for the reflectance. If we assume the absence of other phenomena such as luminescence, it is possible to expect that $T(\lambda) = 0$ when $T_n(\lambda)$ reaches its minimum value, T_{min}. So, p can be evaluated by $p = 1-(T_{min}/T_s)$. By using the calculated values of p into the $T_n(\lambda)$ and $R_n(\lambda)$ equations, we can obtain the reflectance, $R(\lambda)$, and transmittance, $T(\lambda)$, of an ideal/equivalent sample made by a layer of $FeTi_2O_5$ covering the entire surface whose optical parameters, i.e., refractive index $n(\lambda)$ and extinction coefficient $k(\lambda)$, coincide with the mean values of $FeTi_2O_5$. In our case, the covered surface value is about 79 % at T = 560 °C and 73 % at 750 °C.

The curves of the real part of the refractive index, $n(\lambda)$, as estimated from the calculated $T(\lambda)$ and $R(\lambda)$ curves by means of the KSEMAW open-source software, are shown in Fig. 7a. The error bars ($\pm\delta n$) for the refraction index n are also shown. The accuracy in the determination of n is better than ±0.5 % for $\lambda \geq 430$ nm and ±3 % in the range 430–370 nm. Not reliably values of n ($\delta n/n > \pm 9$ %) were obtained for $\lambda < 370$ nm.

In the same figure the absorption coefficients α calculated as $\alpha = 4\pi k/\lambda$, are reported (Fig. 7b). Near the optical band gap energy E_g, the absorption coefficient α should follow the well-known dependence: $\alpha h\nu \approx A(h\nu - E_g)^r$, where A is a sample-dependent constant parameter and r is equal to 1/2 and 2 for direct and indirect allowed transitions, respectively, and hν is the photon energy [48]. If α is plotted versus the energy, a sharp edge should be seen near the E_g value [48]. In our case, instead of a clear and sharp edge, only a weak knee around 2.3 eV can be distinguished (see arrows in Fig. 7b). The $(\alpha h\nu)^{1/r}$ plots versus the photon energy hν of the sample heated in air at 560 °C and at 750 °C are shown in Fig. 8 for both the direct (Fig. 8a) and indirect cases (Fig. 8b). From these plots, no conclusions can be drawn on the nature of the bandgap, since in both cases (r equal to 1/2 or 2) there is an energy region with a linear behavior. In any case, the intercepts of the linear-fit extrapolations with the horizontal axes led us to estimate an energy gap of about 2.25 eV (which is not far away from 2.3 eV) for the sample treated at 560 °C, and a value only slightly higher for the sample treated at 750 °C in the case of indirect transition (Fig. 8b).

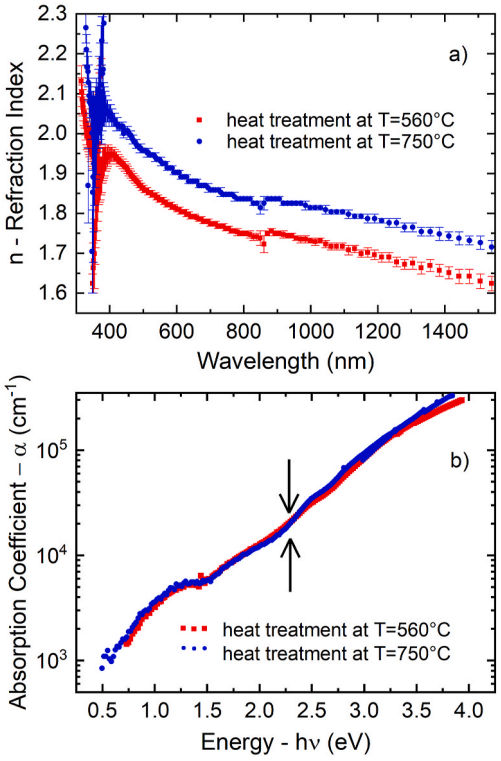

Fig. 7. Refractive index, n, (a) and logarithmic scale of the absorption coefficient ($\alpha = 4\pi k/\lambda$) versus wavelengths, λ, (b) of a sample heat-treated at 560 °C (red curves) and at 750 °C (blue curves). The $n(\lambda)$ and $k(\lambda)$ values were obtained from the calculated $T(\lambda)$ and $R(\lambda)$ curves by using the KSEMAW open-source software. (For interpretation of the references to colour in this figure legend, the reader is referred to the Web version of this article.)

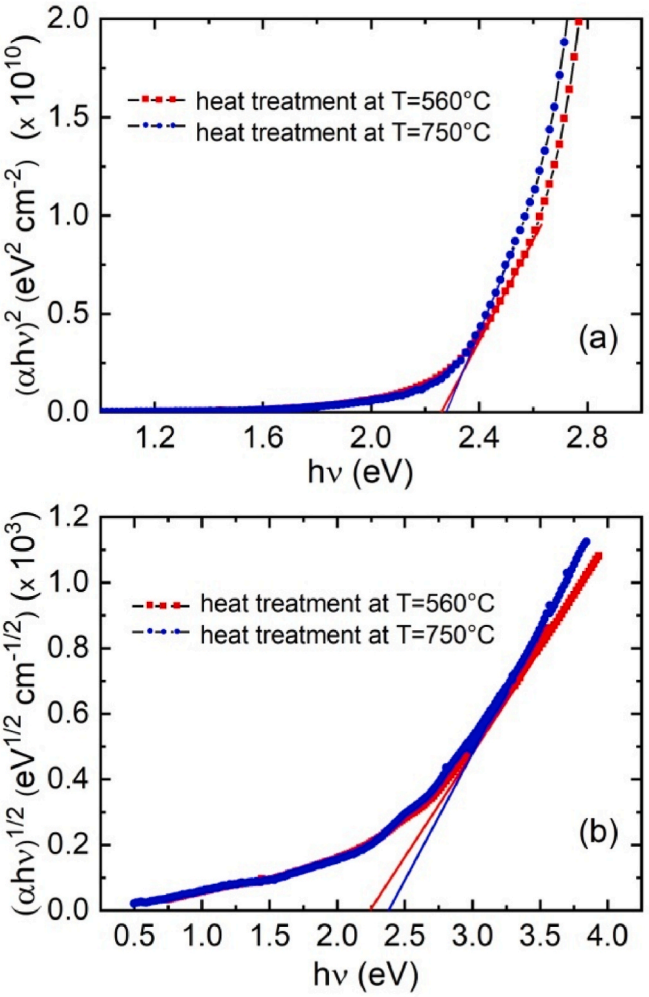

Fig. 8. Dispersion versus photon energy (hν) of $(\alpha h\nu)^2$ (direct transition) (a) and of $(\alpha h\nu)^{1/2}$ (indirect transition) (b) of a sample heat treated at 560 °C (red curves) and at 750 °C (blue curves). The graphical estimation of the energy gap is also reported. (For interpretation of the references to colour in this figure legend, the reader is referred to the Web version of this article.)

Comparing the optical results of the samples annealed at 560 and 750 °C, only minor changes (around 5 %) between the optical parameters can be observed. By increasing the temperature, indeed, the covered surface area reduces from 79 % to 73 %, the equivalent film thickness decreases from 66.0 to 62.5 nm, whereas the refractive index value increases by about 0.1. Since the refractive index is mainly determined by composition, morphology, and structure of the bulk of a sample [50], the slight changes in the optical parameters observed after the heating at 750 °C could be attributed to a higher density of the sample [49] due to the reduction of the equivalent thickness, associated with a likely thickness fluctuation (or thickness gradient) along the surface or by the smaller surface area covered by the coating.

4. Conclusions

High thermally stable wide-bandgap, single-phase ferro-pseudobrookite, $FeTi_2O_5$, polycrystalline coatings were successfully

grown on fused silica and (100)-Si substrates by an optimized sol-gel route using a precursor solution with a molar ratio Fe:Ti = 1:2. We report on the optical properties (determination of the complex refractive index and the energy gap), the effect of the temperature on the chemical, the microstructural characteristics of the $FeTi_2O_5$ crystalline phase, and the underlying causes of the formation of the rutile-TiO_2 secondary phase.

TG-DSC thermal analyses combined with XRD and FTIR investigations showed the formation of a single phase of orthorhombic $FeTi_2O_5$ at 560 °C (crystalline domain size ≈16 nm). Characterization performed on annealed coatings (up to 950 °C) show that the coatings remain in single $FeTi_2O_5$ phase up to a temperature of about 590 °C. At higher temperatures, indeed, superficial Ti-O- dangling bonds begin to arrange themselves to form polycrystalline rutile-TiO_2 (crystalline domain size about 8 nm at 620 °C), while the ferro-pseudobrookite phase remains unchanged. Experimental characterizations performed on sol-gel powders annealed under two different atmospheres, air and argon, show the formation of the secondary phase both in oxidizing and inert atmospheres, demonstrating that the formation of rutile-TiO_2 is due to annealing processes, and it is not influenced by oxygen presence.

The experimental results also suggest that increasing the annealing temperature above 750 °C, the differences in the local chemical environments surrounding Ti and O atoms within the $FeTi_2O_5$ structure decreases, and the energy required to break its Ti-O-Ti molecular bonds increases, consequently increasing the thermal stability of Ti-O-Ti chemical bonds of the $FeTi_2O_5$ crystalline structure.

Optical absorption measurements carried out on films grown by the spin-coating method on silica substrates annealed at 560 °C (pure $FeTi_2O_5$) yield a refractive index of about 1.84 at 550 nm and an optical band gap of about 2.25 eV; a weak positive band peaked at about 5.9 eV seems affecting the transmittance of the samples. Increasing the temperature up to 750 °C, the energy gap remains almost unchanged, whereas the positive band in the transmittance disappears. The slight increase of the refractive index (<5 %) at 750 °C suggests a higher density of the coatings due to the annealing performed at a higher temperature.

The high thermal stability, up to 1140 °C [31], together with a wide band-gap and the absence of any impurity phases up to an operating temperature of about 590 °C, could make $FeTi_2O_5$ a promising wide-bandgap material for the fabrication of power electronic, magneto-electronic and optical-electronic devices, in particular in the field of photocatalysis, photovoltaic and high-temperature thermoelectric applications, and for the green production of hydrogen by water splitting.

CRediT authorship contribution statement

Maria Cristina Ferrara: Writing – review & editing, Writing – original draft, Visualization, Supervision, Investigation, Funding acquisition, Conceptualization. **Marco Montecchi:** Writing – original draft, Visualization, Investigation. **Alberto Mittiga:** Writing – original draft, Visualization, Investigation. **Monica Schioppa:** Visualization, Investigation. **Saverio Mazzarelli:** Visualization, Investigation. **Leander Tapfer:** Writing – review & editing, Writing – original draft, Visualization, Investigation. **Nico Lovergine:** Writing – review & editing, Visualization, Investigation. **Paola Prete:** Writing – review & editing, Visualization, Investigation, Writing – original draft.

Data availability

The main data that support the findings of this study are available within the article. However, all data that support the findings of this study are available from the corresponding author upon reasonable request.

Declaration of generative AI and AI-assisted technologies in the writing process

No generative AI and AI-assisted technologies were used in the writing process.

Declaration of interest statement

The authors declare that they have no known competing financial interests or personal relationships that could have appeared to influence the work reported in this article.

Acknowledgements

The authors wish to thank Rosa Chierchia and Nicola Lisi for useful discussions.

References

[1] H.A. Centurion, M.A. Melo, L.G. Rabelo, G.A.S. Alves, W. Santa Rosa, I. Rodríguez-Gutiérrez, F.L. Souza, R.V. Gonçalves, Emerging trends of pseudobrookite Fe_2TiO_5 photocatalyst: a versatile material for solar water splitting systems, J. Alloys Compd. 933 (2023) 167710, https://doi.org/10.1016/j.jallcom.2022.167710.

[2] H. Li, H. Yamahara, H. Tabata, M. Seki, Epitaxial thin films of room-temperature ferromagnetic semiconductor based on Fe_2TiO_5–$FeTi_2O_5$ solid solution, Appl. Phys. Lett. 119 (2021) 022402, https://doi.org/10.1063/5.0055324.

[3] G. Seitz, N. Penin, L. Decoux, A. Wattiaux, M. Duttine, M. Gaudon, Near the ferric pseudobrookite composition (Fe_2TiO_5), Inorg. Chem. 55 (2016) 2499–2507, https://doi.org/10.1021/acs.inorgchem.5b02847.

[4] M.C. Ferrara S. Mazzarelli, M. Schioppa, L. Pilloni, L. Tapfer, Growth, optical, and wettability properties of iron modified titania and ferropseudobrookite thin films, J. Appl. Phys. 130 (2021) 145301, https://doi.org/10.1063/5.0061017.

[5] K.-M. Min, K.-S. Park, A.-H.- Lim, J.-C. Kim, D.-W. Kim, Synthesis of pseudobrookite-type Fe_2TiO_5 nanoparticles and their Li-ion electroactivity, Ceram. Int. 38 (2012) 6009–6013, https://doi.org/10.1016/j.ceramint.2012.03.044.

[6] M.V. Nikolic, Z.Z. Vasiljevic, M.D. Lukovic, V.P. Pavlovic, J. Vujancevic, M. Radovanovic, J.B. Krstic, B. Vlahovic, V.B. Pavlovic, Humidity sensing properties of nanocrystalline pseudobrookite (Fe_2TiO_5) based thick films, Sens. Actuators B Chem. 277 (2018) 654–664, https://doi.org/10.1016/j.snb.2018.09.063.

[7] S. Halpegamage, Z.-H. Wen, X.-Q. Gong, M. Batzill, Monolayer intermixed oxide surfaces: Fe, Ni, Cr, and V oxides on rutile TiO_2(011), J. Phys. Chem. C 120 (2016) 14782–14794, https://doi.org/10.1021/acs.jpcc.6b05186.

[8] N. Son, J.Y. Do, N.-K. Park, U.S. Kim, J.-I. Baek, D. Lee, H.-J. Ryu, M. Kang, Oxygen transfer capacity of pseudobrookite particles derived from ilmenite mineral (x wt.%CuO/y wt.%red mud-z wt.%ilmenite), J. Nanosci. Nanotechnol. 19 (2019) 6590–6600, https://doi.org/10.1166/jnn.2019.17087.

[9] S. Halpegamage, L. Bignardi, P. Lacovig, K. Al, Z.-H. Wen, X.-Q. Gong, S. Lizzit, M. Batzill, An ordered mixed oxide monolayer formed by iron segregation on rutile-TiO_2(011): structural determination by x-ray photoelectron diffraction, J. Phys. Chem. 120 (2016) 26414–26424, https://doi.org/10.1021/acs.jpcc.6b09651.

[10] M. Osada, K. Nishio, H.Y. Hwang, Y. Hikita, Synthesis and electronic properties of Fe_2TiO_5 epitaxial thin films, Apl. Mater. 6 (2018) 056101, https://doi.org/10.1063/1.5025569.

[11] H. Li, H. Yamahara, H. Tabata, M. Seki, Epitaxial thin films of room-temperature ferromagnetic semiconductor based on Fe_2TiO5–$FeTi2O_5$ solid solution, Appl. Phys. Lett. 119 (2021) 022402, https://doi.org/10.1063/5.0055324.

[12] M. Enhessari, M.K. Razi, L. Etemad, A. Parviz, M. Sakhaei, Structural, optical and magnetic properties of the Fe_2TiO_5 nanopowders, J. Exp. Nanosci. 9 (2014) 167–176, https://doi.org/10.1080/17458080.2011.649432.

[13] L. Jin, C. Zhou, Electronic structures and optic properties of Fe_2TiO_5 using LSDA+U approach, Prog. Nat. Sci.: Mater. Int. 23 (2013) 413–419, https://doi.org/10.1016/j.pnsc.2013.06.012.

[14] C. Chen, B.R. Müller, O.I. Lebedev, F. Giovannelli, G. Bruno, F. Delorme, Effects of impurities on the stability of the low thermal conductivity in Fe_2TiO_5 ceramics, Mater. Char. 149 (2019) 111–117, https://doi.org/10.1016/j.matchar.2019.01.021.

[15] N. Daneu, T. Radosevic, S. Bernik, D. Hanzel, M. Mazaj, M. Macek Krzmanc, D. Verhovsek, A. Kocjan, M. Vrabec, M. Spreitzer, E. Guilmeau, Thermoelectric properties of pseudobrookite-based ceramics prepared from natural Fe-Ti-rich heavy mineral sand concentrate, J. Eur. Ceram. Soc. 43 (2023) 7499–7507, https://doi.org/10.1016/j.jeurceramsoc.2023.07.071.

[16] H.D. Ngo, T.D. Ngo, A. Tamanai, K. Chen, N.T. Cuong, O.S. Handegard, A. Pucci, N. Umezawa, T. Nabatame, T. Nagao, Structure and optical properties of sputter deposited pseudobrookite Fe_2TiO_5 thin films, CrystEngComm 21 (2019) 34–40, https://doi.org/10.1039/C8CE01475B.

[17] H. Kozuka, M. Kajimura, Sol-gel preparation and photoelectrochemical properties of Fe_2TiO_5 thin films, J. Sol. Gel Sci. Technol. 22 (2001) 125–132, https://doi.org/10.1023/A:1011228706934.

[18] P.S. Bassi, S.Y. Chiam, J. Barber Gurudayal, L.H. Wong, Hydrothermal grown nanoporous iron-based titanate, Fe_2TiO_5 for light driven water splitting, ACS Appl. Mater. Interfaces 6 (2014) 22490–22495, https://doi.org/10.1021/am5065574.
[19] Q. Liu, J. He, T. Yao, Z. Sun, W. Cheng, S. He, Y. Xie, Y. Peng, H. Cheng, Y. Sun, Y. Jiang, F. Hu, Z. Xie, W. Yan, Z. Pan, Z. Wu, S. Wei, Aligned Fe_2TiO_5-containing nanotube arrays with low onset potential for visible-light water oxidation, Nat. Commun. 5 (2014) 5122, https://doi.org/10.1038/ncomms6122.
[20] M. Ramezani, A. Davoodi, A. Malekizad, S.M. Hosseinpour-Mashkani, Synthesis and characterization of Fe_2TiO_5 nanoparticles through a sol–gel method and its photocatalyst applications, J. Mater. Sci. Mater. Electron. 26 (2015) 3957–3962, https://doi.org/10.1007/s10854-015-2930-6.
[21] J. Deng, X. Lv, J. Liu, H. Zhang, K. Nie, C. Hong, J. Wang, X. Sun, J. Zhong, S.-T. Lee, Thin-layer Fe_2TiO_5 on hematite for efficient solar water oxidation, ACS Nano 9 (2015) 5348–5356, https://doi.org/10.1021/acsnano.5b01028.
[22] M. Wang, X. Wu, K. Huang, Y. Sun, Y. Zhang, H. Zhang, J. He, H. Chen, J. Ding, S. Feng, Enhanced solar water-splitting activity of novel nanostructured Fe_2TiO_5 photoanode by electrospray and surface F-modification, Nanoscale 10 (2018) 6678–6683, https://doi.org/10.1039/C8NR01331D.
[23] S. Kumari, C. Khare, F. Xi, M. Nowak, K. Sliozberg, R. Gutkowski, P.S. Bassi, S. Fiechter, W. Schuhmann, A. Ludwig, Combinatorial search for new solar water splitting photoanode materials in the thin-film system Fe–Ti–W–O, Z. Phys. Chem. 234 (2020) 867–885, https://doi.org/10.1515/zpch-2019-1462.
[24] J. Hu, S. Zhao, X. Zhao, Z. Chen, Strategies of anode materials design towards improved photoelectrochemical water splitting efficiency, Coatings 9 (2019) 309, https://doi.org/10.3390/coatings9050309.
[25] B. Karimi, M.H. Habibi, High photocatalytic activity of light-driven Fe_2TiO_5 nanoheterostructure toward degradation of antibiotic metronidazole, J. Ind. Eng. Chem. 80 (2019) 292–300, https://doi.org/10.1016/j.jiec.2019.08.007.
[26] M. Osada, K. Nishio, K. Lee, M. Colletta, B.H. Goodge, W.J. Kim, L.F. Kourkoutis, Epitaxial thin film photoanodes, ACS Appl.Ener.Mater. 4 (2021) 2098–2106, https://doi.org/10.1021/acs.jpcc.8b11479.
[27] K. Chen, T.D. Dao, T.D. Ngo, H.D. Ngo, A. Tamanai, S. Ishii, X. Li, H. Misawa, T. i Nagao, Enhanced photocurrent generation from indium–tin-oxide/Fe_2TiO_5 hybrid nanocone arrays, Nano Energy 76 (2020) 104965, https://doi.org/10.1016/j.nanoen.2020.104965.
[28] P.S. Bassi, F. Xi, M. Kölbach, R. Gunder, I. Ahmet, R. van de Krol, S. Fiechter, Pulsed laser deposited Fe_2TiO_5 photoanodes for photoelectrochemical water oxidation, J. Phys. Chem. C 124 (2020) 19911–19921, https://doi.org/10.1021/acs.jpcc.0c04396.
[29] Hao-Hang Xu, J. Liu, L.L. Tao, Xian-Jie Wang, S.V. Streltsov, Yu Sui, Possible spin Jahn-Teller material: ordered pseudobrookite $FeTi_2O_5$, Phys. Rew. B 109 (2024) 184430, https://doi.org/10.1103/PhysRevB.109.184430.
[30] F. Lang, L. Jowitt, D. Prabhakaran, R.D. Johnson, S.J. Blundell, $FeTi_2O_5$: a spin Jahn-Teller transition enhanced by cation substitution, Phys. Rev. B 100 (2019) 094401, https://doi.org/10.1103/PhysRevB.100.094401.
[31] I.J. Kim, L.J. Gauckler, Formation, decomposition and thermal stability of Al_2TiO_5 ceramics, J. Ceram. Sci. Technol. 3 (2012) 49–60, https://doi.org/10.4416/-00049.
[32] H.Z. Massoud, The onset of the thermal oxidation of silicon from room temperature to 1000°C, Microelectr. Eng. 28 (1995) 109–116, https://doi.org/10.1016/0167-9317(95)00026-5.
[33] M. Montecchi, A. Mittiga, C. Malerba, F. Menchini, F. Ksemaw, An open-source software for the analysis of spectrophotometric, ellipsometric and photothermal deflection spectroscopy measurements, Open Res 1 (Europe 2023) 95, https://doi.org/10.12688/openreseurope.13842.2.
[34] Haike Wanga, Hui Qiana, Yanyan Gaoa, Yabin Lic, Classification and physical characteristics of bound water in loess and its main clay minerals, Eng. Geol. 265 (2020) 105394, https://doi.org/10.1016/j.enggeo.2019.105394.
[35] H. Müller-Buschbaum, M. Waburg, Pseudobrookite mit weitgehend geordneter Metallverteilung: $CoTi_2O_5$, $MgTi_2O_5$ und $FeTi_2O_5$, Monatsh. Chem. 114 (1983) 21–25, https://doi.org/10.1007/BF00809371.
[36] W.Q. Guo, S. Malus, D.H. Ryan, Z. Altounian, Crystal structure and cation distribution in the $FeTi_2O_5$-Fe_2TiO5 solid solution series, J. Phys. Condens. Matter 11 (1999) 6337–6346, https://doi.org/10.1088/0953-8984/11/33/304.
[37] Jcpds - ICDD—international centre for diffraction data. http://www.icdd.com/, 2000.
[38] V.A. Zeitler, C.A. Brown, The infrared spectra of some Ti-O-Si, Ti-O-Ti and Si-O-Si compounds, J. Phys. Chem. 61 (1957) 1174–1177, https://doi.org/10.1021/j150555a010.
[39] D.C. Leite Vasconcelos, V.C. Costa, E.H.M. Nunes, A.C. Soares Sabioni, M. Gasparon, W.L. Vasconcelos, Infrared spectroscopy of titania sol-gel coatings on 316L stainless steel, Mater. Sci. Appl. 2 (2011) 1375–1382, https://doi.org/10.4236/msa.2011.210186.
[40] Samya El-Sherbiny Fatma Morsy, Marwa Samir, A. Osama, Fouad, Synthesis, characterization and application of TiO_2 nanopowders as special paper coating pigment, Appl. Nanosci. 4 (2014) 305–313, https://doi.org/10.1007/s13204-013-0196-y.
[41] V.G. Erkov, S.F. Devyatova, E.L. Molodstova, T.V. Malsteva, U.A. Yanovskii, Si–TiO_2 interface evolution at prolonged annealing in low vacuum or N_2O ambient, Surf. Sci. 166 (2020) 51–56, https://doi.org/10.1016/S0169-4332(00)00415-3.
[42] Th Posch, F. Kerschbaum, D. Fabian, H. Mutschke, J. Dorschner, A. Tamanai, Th Henning, Infrared properties of solid titanium oxides: exploring potential primary dust condensates, Astrophys. J. Suppl. 149 (2003) 437–445, https://doi.org/10.1086/379167.
[43] M. Johnson, M. Ates, Z. Arslan, I. Farah, C. Bogatu, Assessment of crystal morphology on uptake, particle dissolution, and toxicity of nanoscale titanium dioxide on artemia salina, J. Nanotox. Nanomed. 2 (2017) 11–27, https://doi.org/10.4018/JNN.2017010102.
[44] S.J.M. Marshall, M.R. Castell, Shape transitions of epitaxial islands during strained layer growth: anatase TiO_2 on $SrTiO_3$, Phys. Rev. Lett. 102 (2009) 146102.
[45] M.S.J. Marshall, A.E. Becerra-Toledo, L.D. Marks, M.R. Castell, Defects on strontium titanate, in: J. Jupille, G. Thornton (Eds.), Chapter 11 in “Defects at Oxide Surfaces”, vol. 58, Springer Ser. Surf. Sci, 2015, pp. 327–349, https://doi.org/10.1103/PhysRevLett.102.146102.
[46] F. Silly, M.R. Castell, Formation of single-domain anatase TiO_2 (001) -(1x4) islands on $SrTiO_3$(001) after thermal annealing, Appl. Phys. Lett. 85 (2004) 3223–3225, https://doi.org/10.1063/1.1805177.
[47] K.V. Ivanov, A.V. Noskov, O.V. Alekseeva, A.V. Agafonov, Effect of annealing conditions on the physicochemical and photocatalytic properties of a nanopowder based on Fe2TiO5, Mater. Chem. Phys. 299 (2023) 127493, https://doi.org/10.1016/j.matchemphys.2023.127493.
[48] L. Haryński, A. Olejnik, K. Grochowska, K. Siuzdak, A facile method for Tauc exponent and corresponding electronic transitions determination in semiconductors directly from UV–Vis spectroscopy data, Opt. Mater. 127 (2022) 112205, https://doi.org/10.1016/j.optmat.2022.112205.
[49] M.C. Ferrara, L. Pilloni, S. Mazzarelli, L. Tapfer, Hydrophilic and optical properties of nanostructured titania prepared by sol–gel dip coating, J. Phys. D Appl. Phys. 43 (2010) 095301, https://doi.org/10.1088/0022-3727/43/9/095301.